Drifts and Environmental Disturbances in Atomic Clock Subsystems: Quantifying Local Oscillator, Control Loop, and Ion Resonance Interactions

Daphna G. Enzer, William A. Diener, David W. Murphy, Shanti R. Rao, and Robert L. Tjoelker, *Senior Member, IEEE*

***Abstract*— Linear ion trap frequency standards are among the most stable continuously operating frequency references and clocks. Depending on the application, they have been operated with a variety of local oscillators (LOs), including quartz ultrastable oscillators, hydrogen-masers, and cryogenic sapphire oscillators. The short-, intermediate-, and long-term stability of the frequency output is a complicated function of the fundamental performances, the time dependence of environmental disturbances, the atomic interrogation algorithm, the implemented control loop, and the environmental sensitivity of the LO and the atomic system components. For applications that require moving these references out of controlled lab spaces and into less stable environments, such as fieldwork or spaceflight, a deeper understanding is needed of how disturbances at different timescales impact the various subsystems of the clock and ultimately the output stability. In this paper, we analyze which perturbations have an impact and to what degree. We also report on a computational model of a control loop, which keeps the microwave source locked to the ion resonance. This model is shown to agree with laboratory measurements of how well the feedback removes various disturbances and also with a useful analytic approach we developed for predicting these impacts.**

***Index Terms*— Atomic clocks, atomic frequency standards, local oscillators (LOs).**

I. Introduction

LINEAR ion trap clocks promise to be a new next generation of highly stable, robust frequency standards for a range of laboratory, fieldwork, and space applications [1]–[5]. The National Aeronautics and Space Administration (NASA) can benefit from their long-term stability as a complement to the maser-based frequency standards in their deep space network [6] and/or as a new one-way navigation tool for future flight missions [7], [8]. The Deep Space Atomic Clock mission (DSAC) is a flight demonstration aimed to validate operation of a room temperature Hg ion clock in space and to lay the foundation for future missions that would rely on such a stable onboard clock [5], [8].

The most stable Hg ion clocks rely on the long-term stability of the ions' resonant frequency coupled with the superior short-term performance of state-of-the-art local oscillators (LOs) [1]. Long-term stability is often thought of as being determined by the absolute stability of the atomic reference. However, in truth, it results from a more complicated interaction between the LO, atomic reference, and interrogation approach. A control loop measures and corrects the long-term behavior of the LO, but not surprisingly, sensitivities remain to temperature, magnetic field, interrogation duty cycle, and control loop aggressiveness. Environmental impacts on atomic and LO components are often mitigated by magnetic shielding and temperature control, but here, we present a unified picture for evaluating the Allan deviation (ADEV) impact due to the remaining sensitivities. In particular, we show a direct correlation between changes in LO frequency drift rate and changes in clock output frequency. This is to be distinguished from the well-known Dick effect [9], [10], which is most commonly interpreted as the aliasing of oscillator noise into long-term output noise.

In this paper, we quantify the impact of periodic disturbances to the LO, to the frequency generation subsystem, and to the atomic resonance, as well as the impact of a weakly nonlinear LO frequency drift. In the case of periodic LO disturbance, we quantify the common conception that the impact is mostly removed by the control loop. In addition, we clarify which disturbances cancel and which ones add when impacts are common to different elements in the frequency chain. And finally, we present how to predict the impact of fast nonperiodic disturbances that have slower periodic envelopes, with particular attention to whether they occur during the microwave interrogation or during the portion of the clock cycle when the microwave probe is OFF.

II. Ion Clock System

Fig. 1 shows the simplest LO-atomic system architecture, used in prior Hg ion clock implementations at the Jet Propulsion Laboratory (JPL) [1]–[4]. It shows an LO feeding a 40-GHz synthesizer that probes the ion resonance. Feedback to the LO assures that the 40 GHz remains resonant with the ion clock transition. A variant of this system architecture, shown in Fig. 2, was recently used for DSAC [5], [8]. It consists of an LO feeding a 40-GHz synthesizer that probes the ion resonance, but also feeding a 10- or 20-MHz synthesizer, which serves as the User Output. Adding a User

Manuscript received September 10, 2016; accepted November 30, 2016. Date of publication December 19, 2016; date of current version March 1, 2017. This work was supported in part by the Jet Propulsion Laboratory, California Institute of Technology, and in part by the National Aeronautics and Space Administration.

The authors are with the Jet Propulsion Laboratory, California Institute of Technology, Pasadena, CA 91109 USA (e-mail: daphna.g.enzer@jpl.nasa.gov).

Digital Object Identifier 10.1109/TUFFC.2016.2636088

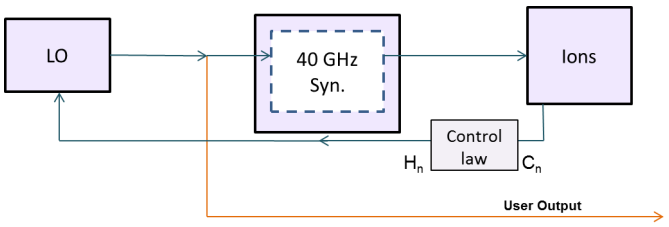

Fig. 1. Typical block diagram of a linear ion trap clock. The LO feeds the 40-GHz synthesizer, which is used to probe the ion resonance, and it also serves as the User Output. Control loop corrections are applied directly to the LO.

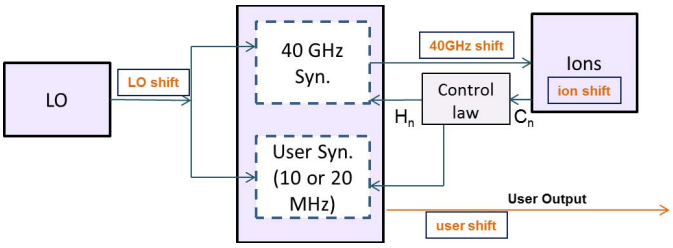

Fig. 2. Block diagram of clock for the DSAC implementation. The LO feeds the 40-GHz synthesizer, and also feeds the 10- or 20-MHz User Output synthesizer. Control loop corrections are applied to both synthesizers simultaneously, mimicking the direct feedback architecture of Fig. 1. However, the separation of the LO's two functions across these two synthesizers introduces the possibility of new environmental impacts that would not be present in a direct feedback system. The four boxes labeled as shifts represent the locations we insert environmental disturbances in our experimental tests and/or computer simulations.

Output synthesizer is a compromised implementation of feedback and adds some complexity for understanding the impact of disturbances. This paper focuses on the more general block diagram, Fig. 2, noting that the results presented here can be simplified to the direct feedback system of Fig. 1 by zeroing the disturbances on the User Output synthesizer.

Depending on the application, ion clocks have been operated with a variety of LO's, including quartz ultrastable oscillators (USOs), hydrogen masers, and cryogenic sapphire oscillators. Ion clock implementations at JPL have also differed in terms of whether they operate within quadrupole or multipole ion traps. Multipole trap operation usually relies on a quadrupole trap for ion loading, but then ions are shuttled to the more isolated multipole region for the crucial microwave interrogation portion of the cycle. Each clock interrogation cycle consists of several steps that include ion loading, state preparation, microwave interrogation (of the Rabi variety for this paper), state detection, LO frequency correction, and possibly ion shuttling between traps. Differences in clock cycle time between quadrupole versus multipole clock operation will impact the effectiveness of the control loop in removing some environmental disturbances.

Experimental data in this paper were obtained from a legacy linear ion trap standard (LITS) quadrupole Hg ion clock in JPL's Frequency Standards Test Lab that was adapted to add a direct digital synthesizer (DDS)-based User Output synthesizer, as shown in Fig. 2. The LITS had a built-in voltage controlled crystal oscillator (VCXO) as an LO [1] with a high precision time-analog-converter (TAC) implementation to directly steer the VCXO [11]. To mock up the DSAC configuration shown in Fig. 2, we held the VCXO fixed and instead applied error corrections on the User Output via a low noise commercial DDS. The VCXO and TAC system has a drift compensation system that enabled us to tune out much of the crystal frequency drift or dial in a larger than normal drift when desired. Computer model results presented in this paper are based on the adapted LITS/VCXO clock operation parameters or on DSAC design parameters. DSAC has a quadrupole and multipole trap and also operates with a USO as the LO [5].

III. Control Loop

The control loop studied in the adapted LITS/VCXO clock and also the one modeled is based on that used in years of operating linear ion trap clocks at JPL, but with an improved drift compensation algorithm. The microwave probe frequency is square-wave modulated from one side of the Rabi resonance to the other side during each successive interrogation cycle, and the photons scattered from the trapped ions are detected, and then the control law is applied.

The first step in the control law is to convert the nth detected photon count C_n into an error signal E_n that estimates the hyperfine state of the clock over the past few cycles. This stage and the next, a filtering stage, can be described by the discrete-time transfer function [12]

$$F(z) = \frac{1}{2} \cdot \frac{1 + 2z^{-1} + 1z^{-2}}{1 + 0.75z^{-1} + 0.25z^{-2}}$$

where $z = e^{i(2\pi f)T_s}$, f is the disturbance frequency, and T_s is the clock cycle period. The coefficients of the z^{-1} terms in this function are chosen in two stages so that, overall, it approximates a low-pass filter.

First, the numerator is implemented as the difference function $E_n = (-1)^n (C_n - 2C_{n-1} + C_{n-2})$. This set of coefficients, $\{1, 2, 1\}$, can be thought of as a "window" function for averaging the C_n observations, alternating the sign for each coefficient at each sample to compensate for the alternating slope of the Rabi curve on successive cycles. Note that other window functions that have been used include $\{1, 1\}$ and $\{1, 3, 3, 1\}$. The former, acting on fewer samples, averages the behavior of the clock over two cycles, while the latter averages over four cycles. While an infinite number of window functions exist, these have the properties that they are symmetric in time and the sum of the even (n and $n-2$) coefficients is equal and opposite to the odd coefficients ($n-1$ and $n-3$), making the error signal much less sensitive to changes in the background light level that may result from, for example, fluctuations in the light source output or the number of trapped ions in the clock.

Next, the coefficients of the denominator are chosen to make the overall effect of $F(z)$ be, for the $\{1, 2, 1\}$ window choice, an approximation to a second-order Butterworth low-pass filter [13]. With our coefficient choices, the cutoff frequency is approximately $1/(3T_s)$. This second stage of the control law is implemented with the difference equation $F_n = E_n - 0.75F_{n-1} - 0.25F_{n-2}$.

These two difference equations (E_n and F_n) are adequate, with an appropriate scaling factor, to provide an adjustment to

the synthesizers that enables the clock to function. However, to suppress the effect of LO disturbances with longer characteristic timescales, we add another optional layer of filtering, the "drift compensator." An integrating filter could be used to suppress static offset errors [14], but for the circumstance where the systematic errors are changing slowly, we choose a lag compensator [13], with a transfer function

$$H(z) = \frac{1 - 0.975z^{-1}}{1 - 0.9987z^{-1}}.$$

This particular filter can be implemented with the pair of difference equations, $H_n = G_n - 0.975G_{n-1}$, and $G_n = F_n + 0.9987G_{n-1}$.

Opting for drift compensation allows the control loop to anticipate LO drift based on the past history in order to drive the error signal E_n closer to zero bias, without overweighting drift that happened weeks or months ago. Whereas an integrator's gain increases at lower frequencies (and longer timescales), the lag compensator's gain is limited to a maximum gain, which can be determined by setting $z = 1$ (in this case, 19). Drift compensation is used for all tests in this paper unless otherwise specified.

IV. Clock System Model

The generic clock system model was created to simulate how well the control loop is able to respond to LO noise, LO drift, and environmental disturbances, for various choices of clock operation parameters. The algorithm begins by generating a time sequence for LO noise composed of white frequency, white phase, and flicker frequency noise. This LO time sequence is designed to result in a typical and expected ADEV for the LO being modeled. In addition, a linear and quadratic frequency drift is added to the noise sequence.

This LO noise plus drift, expressed as a series of frequencies, is applied to both the microwave and to the User synthesizer, as shown in Fig. 2. The code then evaluates the probability of the 40-GHz probe synthesizer driving a Rabi transition for each clock cycle and generates a detected photon count based on this probability and background photon shot noise. The probability calculation uses the Rabi lineshape equation and a weighted average of microwave frequencies over that cycle's interrogation. The weighting function is discussed in [9] and [10] and is approximated in our algorithm by $\sin^2(\pi t/T_R)$, where t is the time within the microwave interrogation and T_R is the total length of the interrogation (Rabi time).

From this point, the simulation proceeds with the same control law as the physical clock, generating an error signal and a feedback estimate. Feedback is applied to both synthesizers of Fig. 2, based on the presumed difference between the LO and the ion resonance frequency and all the loop filtering and optional drift compensation. As well, the microwave frequency is switched to the other side of resonance. Output of the code is the User synthesizer frequency and its associated ADEV. Frequency disturbances can then be added at any of the locations of Fig. 2 labeled in orange with the word "shift." The input clock parameters to the model are average clock signal counts, average background counts, clock cycle time, and Rabi time.

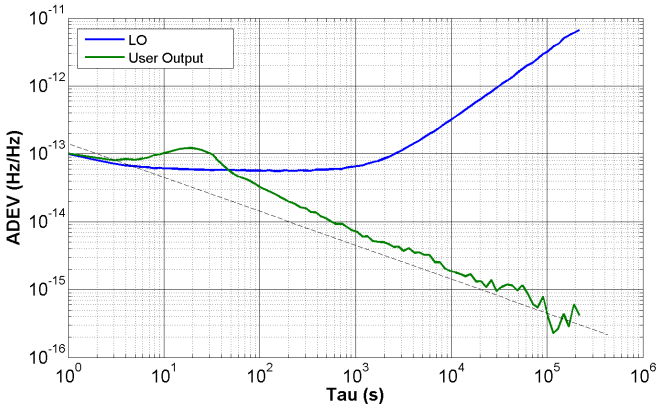

Fig. 3. Simulated LO input (blue) and User Output (green) for typical LITS/VCXO clock parameters. The straight line is the ADEV we would expect from signal to noise alone (no Dick effect or other excess noise): $1.4 \times 10^{-13}/\sqrt{\tau}$ in this case.

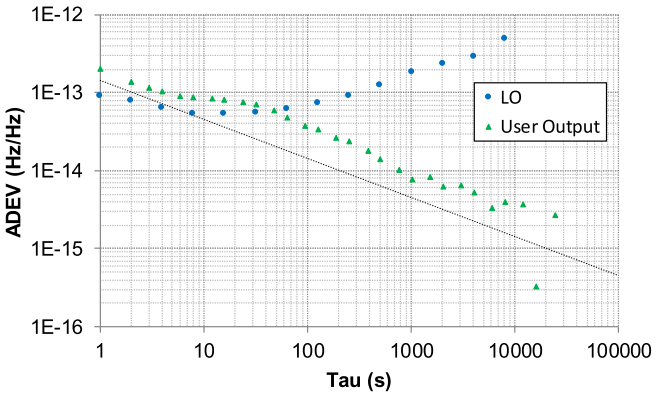

Fig. 4. Experimental LO input (blue circles) and User Output (green triangles) for LITS/VCXO clock modified with a DDS user output. The User Output's ADEV value at 1 s is a bit degraded due to known limitations of the particular User Output synthesizer in this implementation of Fig. 2. Because one microhertz resolution was desired, our choice of synthesizer was limited. However, excess User synthesizer noise does not impact the feedback to the 40-GHz synthesizer, so does not fold into higher tau ADEV values as 1 s LO noise would (Dick effect). The straight line is the ADEV we would expect from signal to noise alone (no Dick effect or other excess noise): $1.4 \times 10^{-13}/\sqrt{\tau}$ in this case.

Fig. 3 shows model results for the LITS/VCXO clock parameters, and Fig. 4 shows the experimental User Output from the commercial 10-MHz DDS card. This provides reasonable validation of the model and enables us to use the model to make predictions for different types of disturbances on the LITS and/or other clock platforms.

V. Paradigm for Understanding Impact of Slow Disturbances

A. Introduction: Analytic Estimate of Allan Deviation Impact Due to Slow Periodic Disturbances

The DSAC flight demonstration will occur in low-earth orbit, and the clock will typically experience variations in temperature and/or magnetic field due to the 98-min orbital period. For DSAC or any generic Hg ion clock, the elements of

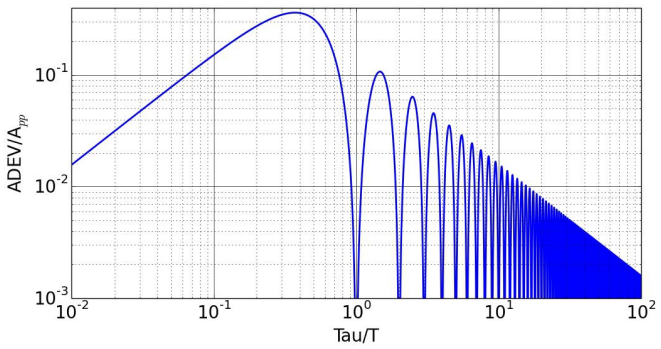

Fig. 5. ADEV of periodic disturbance given by (1).

the system for which we must track thermal/magnetic or other environmental impacts are: 1) the LO/USO; 2) the 40-GHz synthesizer; 3) the ion resonance frequency; and 4) the User Output synthesizer, as labeled in Fig. 2. There is no difference between frequency shifts of the 40-GHz synthesizer and shifts of the ion resonance frequency (other than an important minus sign). Thus, we only need to analyze the impact on three systems: the LO, the ion frequency, and the User Output synthesizer, and then after the fact, use what we learn about ion frequency variation to also include the impact due to 40-GHz synthesizer variations. We provide this system analysis for the configuration shown in Fig. 2 in Sections V-B, V-C, and V-D.

To predict the impact of periodic disturbances on the ADEV curve, we evaluate the ADEV [15] of a frequency disturbance $y_{\text{dist}}(t)$ with peak-to-peak magnitude A_{pp} and period T

$$y_{\text{dist}}(t) = \frac{A_{\text{pp}}}{2}\cos\left(\frac{2\pi t}{T}\right) \tag{1}$$

which can also be considered the result of a phase disturbance

$$x_{\text{dist}}(t) = \frac{A_{\text{pp}}}{2}\frac{T}{2\pi}\sin\left(\frac{2\pi t}{T}\right). \tag{2}$$

The ADEV of this disturbance is calculated to be

$$\sigma_y(\tau) = \frac{A_{\text{pp}}}{2}\left[\sin^2\left(\frac{\pi\tau}{T}\right)\right]\Big/\frac{\pi\tau}{T} \tag{3}$$

and is shown in Fig. 5.

In order to ultimately track the impact of these disturbances with simple formulae, we approximate the shape of this disturbance ADEV by a rising edge, a peak, and a falling edge. For $\tau \ll T$, the rising edge can be approximated by the upper envelope

$$\sigma_y(\tau) = (A_{\text{pp}}/2)(\pi\tau/T). \tag{4}$$

The peak

$$\sigma_y(\tau_{\text{peak}}) \approx 0.36 * A_{\text{pp}} \tag{5}$$

occurs at

$$\tau_{\text{peak}} \approx 0.37 * T. \tag{6}$$

And finally, for $\tau \gg T$, the falling edge can be approximated by the upper envelope

$$\sigma_y(\tau) = \left(\frac{A_{\text{pp}}}{2}\right)\left(\frac{T}{\pi\tau}\right). \tag{7}$$

In many applications, this disturbance ADEV falls below the clock system ADEV for averaging times far from the peak, so to understand environment impacts, often all that is needed is to track the peak ADEV and the tau at which it occurs, i.e., (5) and (6). This simplifies the process greatly and allows for simple analytic estimates of slow disturbance impacts. For example, diurnal signatures with which clock operators are very familiar occur at $\tau_{\text{peak}} = 0.37 * T = 32000$ s according to (6).

B. Slow User Output Synthesizer and/or Ion Resonance Frequency Disturbances

Slow variations of the User synthesizer and/or of the ion resonance frequency are the easiest to understand because, to the first order, they are not filtered out by the control loop and fractional frequency changes of either directly propagate to the User Output.

Understanding why this is so for the "out of loop" User synthesizer is clear by considering the logical layout of the block diagram in Fig. 2. If the User synthesizer shifts frequency, the control loop (which aims to keep the 40-GHz synthesizer resonant with the ions) does not detect anything. No correction is applied and the frequency change of the synthesizer is directly propagated to the User Output.

Similarly, ion resonance frequency shifts propagate directly to the output. Imagine the ion resonance frequency goes up. The control loop, which relies on the frequency difference between the ions and the LO, concludes that the LO frequency went down and adjusts the 40 GHz and the User Output frequencies up the same fractional amount to compensate. Thus, the microwaves are maintained on resonance with the ions and the output tracks the original ion frequency change.

Using the knowledge that slow fractional frequency changes on the User synthesizer and/or the ion resonance frequency propagate directly to the output, and with the analytic estimates of (5) and (6), we now present comparisons of this analytic method with computer simulation results. We program the model with 98-min period sine-wave thermal disturbances in the form of (1), having peak-to-peak amplitude of either $A_{\text{pp}} = 4.9 \times 10^{-13}$ or $A_{\text{pp}} = 4.9 \times 10^{-14}$. These correspond, for example, to thermal sensitivities of 10^{-13}/°C or 10^{-14}/°C, and an assumed 4.9 °C peak-to-peak temperature swing. The analytical prediction of (5) and (6) gives location and heights of the resultant ADEV peaks as $\tau_{\text{peak}} \approx 2200$ s, and $\sigma_y(\tau_{\text{peak}}) \approx 1.8 \times 10^{-13}$ or 1.8×10^{-14}, respectively. In comparison, the simulation results are shown in Fig. 6. The location and height of the disturbance peaks visually agree with analytical prediction, remembering the need to root-square-sum the predicted peak height with the baseline ADEV value. For the larger disturbance, the envelope of the ringing is seen to fall as $1/\tau$. As expected, Fig. 6 shows the same impact whether this disturbance is applied to the User

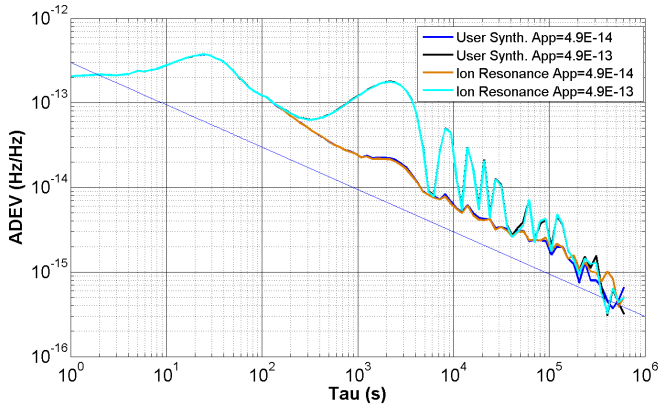

Fig. 6. Simulation results for impact due to two different sized disturbances, applied to either the DSAC User Output synthesizer or ion resonance frequency. The ADEV impact is the same whether the disturbance is applied to the User synthesizer (dark blue and black) or to the ion resonance frequency (orange and teal), as predicted. The straight line is the ADEV we would expect from signal to noise alone (no disturbances, Dick effect or other excess noise): $3 \times 10^{-13}/\sqrt{\tau}$ in this case.

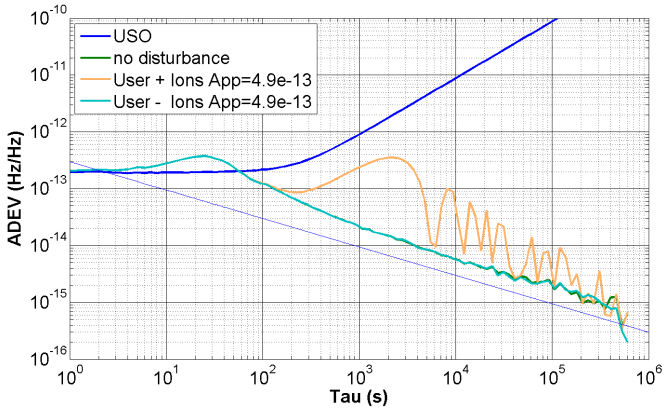

Fig. 7. Simulation results for the larger disturbance of Fig. 6, this time applied to *both* User Output synthesizer *and* ion resonance frequency at the same time. The orange and teal ADEV curves show the impact of applying these frequency disturbances with the same versus opposite polarities. The opposite polarity case (teal) shows the cancelation of the disturbance, resulting in an ADEV that lies on the top of the undisturbed case (green), as predicted. The straight line is the ADEV we would expect from signal to noise alone (no disturbances, Dick effect or other excess noise): $3 \times 10^{-13}/\sqrt{\tau}$ in this case.

synthesizer or to the ion resonance frequency. To verify this point further, Fig. 7 shows the cancelation of the larger of the two disturbances when applied to *both* the User synthesizer *and* ion resonance frequencies with opposite polarities and doubling when applied with the same polarity.

C. Slow LO Disturbances

Slow variations of the LO are more complicated to analyze. To the first order, they are removed by the control loop, but the second order effects cannot be ignored. Referring to the logical layout of Fig. 2, slow drifts in LO frequency are suppressed by the high dc gain of the control loop, which adjusts the two synthesizer outputs to compensate. However, a small bias remains on the output—a static frequency shift that is proportional to the LO frequency drift rate.

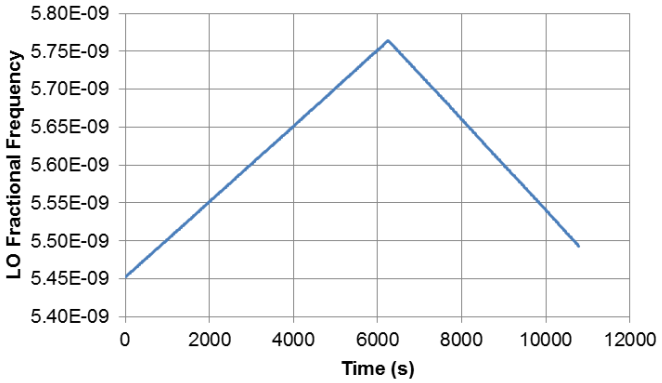

Fig. 8. Data showing LITS LO (VCXO) frequency output when overcompensated to drift fast in a positive direction and then switched to a fast negative drift.

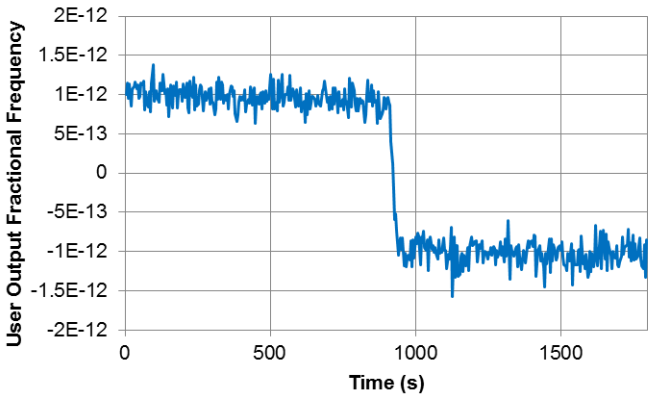

Fig. 9. LITS/VCXO results showing output frequency shift due to abrupt change of LO drift rate from $+5 \times 10^{-9}$/day to -5×10^{-9}/day. No drift compensation implemented for this test.

A fixed-rate drift on the LO, even as large as 10^{-8}/day, appears on the output as a constant frequency offset and does not impact the ADEV. Simulations confirm this. However, if we abruptly *change* the LO drift-rate by 10^{-8}/day, e.g., from $+5 \times 10^{-9}$/day to -5×10^{-9}/day (Fig. 8), the frequency bias changes and we experimentally see this as a shift in the output frequency (Figs. 9 and 10). These tests were performed using the LITS/VCXO system described earlier. The drift rate change from $+5 \times 10^{-9}$/day to -5×10^{-9}/day was accomplished by abruptly adjusting its (TAC) drift compensation system [11] from maximum to minimum settings.

Fig. 9 shows the clock output without drift compensation in the control loop, while Fig. 10 shows it with drift compensation. Observe from Fig. 10 that drift compensation does not eliminate the initially large downward 1.8×10^{-12} shift, but it does reduce it by a factor of 9 after several 300-s $1/e$ times, resulting in a final shift of $\sim 2.0 \times 10^{-13}$. A computer simulation (not shown) using LITS/VCXO parameters produces similar results (within 30%) (a shift of 1.4×10^{-12} without drift compensation and the same size shift with drift compensation reducing to 2.5×10^{-13} after several 300-s $1/e$ times). Therefore, these tests not only quantify the impact of changing LO drift-rate, but also characterize

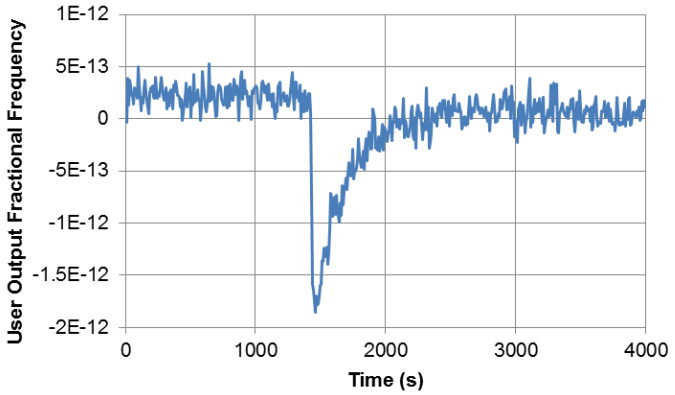

Fig. 10. LITS/VCXO results showing output frequency shift due to abrupt change of LO drift rate from $+5 \times 10^{-9}$/day to -5×10^{-9}/day. Drift compensation implemented for this test.

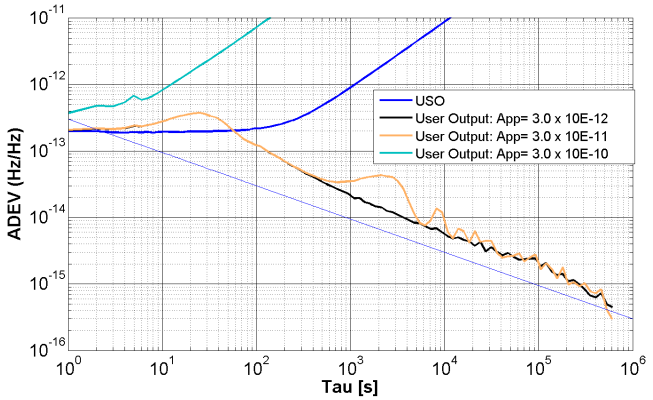

Fig. 11. Simulation results for impact due to three different sized 98-min periodic disturbances, applied to the DSAC USO. The ADEV impacts are smaller than for identical disturbances applied to the User synthesizer or the ion resonance frequency, as expected. The straight line is the ADEV we would expect from signal to noise alone (no disturbances, Dick effect or other excess noise): $3 \times 10^{-13}/\sqrt{\tau}$ in this case. Dark blue curve: USO noise input. Black, orange, and teal curves: simulated clock output.

the advantage of LO drift compensation in the control loop algorithm. For LITS/VCXO clock parameters, with drift compensation, the figure of merit is conservatively taken to be the following output shift per change in LO drift rate: 2.5×10^{-13} shift, per $(10^{-8}$/day) change in LO drift. This figure of merit can be simplified and understood as LITS/VCXO's key sensitivity to LO drift rate

$$dy_{\text{out}}/d\dot{y}_{\text{LO}} = 2.5 \times 10^{-5} \text{ per day}^{-1} = 2.2 \text{ s}. \tag{8}$$

Importantly, this sensitivity to changes in $\dot{y}_{\text{LO}}(t)$ allows us to predict the impact of periodic variations and nonlinear long-term drifts in the LO frequency for DSAC or generic passive frequency standards. In addition, comparison of the sensitivity measurement with and without drift compensation allows for the characterization of the compensation's effectiveness as illustrated by the factor of 6 to 9 reduction in long-term impact of the disturbance of Fig. 8.

As an example of periodic disturbances, we consider a 98-min DSAC orbital thermal variation similar to the one in Section V-B, but this time applied to the LO. Starting with an LO disturbance $y_{\text{LO}}(t)$ described by (1), we calculate an effective disturbance $y_{\text{eff}}(t)$, after filtering by the control loop, by multiplying the DSAC sensitivity analogous to (8) with the LO drift rate $\dot{y}_{\text{LO}}(t)$ to get

$$y_{\text{eff}}(t) = -\frac{A_{\text{pp}}}{2}\frac{2\pi}{T}(2.6 \text{ s}) \sin\left(\frac{2\pi t}{T}\right). \tag{9}$$

Here, we have used the sensitivity 2.6 s, determined by simulating the DSAC system which has different timing parameters due to shuttling into the multipole section of the clock. Comparing (9) to (1), we see that the effective LO disturbance is reduced by $2.6 \text{ s} * 2\pi/T = 0.0028$, and shifted in phase by $-90°$. This reduction factor describes the effectiveness of the control loop, including the drift compensation component. Without drift compensation, this 0.0028 factor would be five times larger. Fig. 11 shows computer simulation results for such a thermal disturbance with peak-to-peak amplitude 3.0 °C (the expected orbital temperature variation at the DSAC USO), and for USO thermal sensitivity cases of 10^{-10}/°C, 10^{-11}/°C, and 10^{-12}/°C. Peak-to-peak disturbance inputs are thus $A_{\text{pp}} = 3.0 \times 10^{-10}$, 3.0×10^{-11}, and 3.0×10^{-12}, and predicted location and heights of the disturbance peaks from (5) and (6) are $\tau_{\text{peak}} \approx 2200$ s, and $\sigma_y(\tau_{\text{peak}}) \approx 3.0 \times 10^{-13}$, 3.0×10^{-14}, and 3.0×10^{-15}.

The largest-sensitivity case (10^{-10}/°C) is shown in teal as the unstable curve for which the simulated clock lost lock. This computational outcome may or may not be fully representative of an actual clock, but serves as a reminder that even if the analytic models do not predict a large impact on ADEV, the disturbances may still be too large to operationally maintain lock. (The analytic predictions (4)–(7) assume that the clock remains locked.) Clocks lose lock when disturbances are so big that feedback takes the new applied frequency too far from resonance so that future corrections have the wrong polarity and drive the probe still further from resonance rather than toward it. Meanwhile, the smallest sensitivity case (the expected sensitivity of the DSAC USO) is shown in black and shows no impact, as expected for the 3.0×10^{-15} prediction at $\tau_{\text{peak}} \approx 2200$ s. Finally, the 10^{-11}/°C sensitivity predicts an ADEV impact of 3.0×10^{-14}, which when root-sum-squared with the 1.3×10^{-14} baseline near 2200 s gives 3.3×10^{-14}, within 20% of the 4.0×10^{-14} value read from the plot.

In the conclusion, we have empirically determined a sensitivity to $\dot{y}_{\text{LO}}(t)$ both through experimental test and through simulation. We have illustrated how to use this sensitivity to calculate a reduction factor that quantifies the filtering of the control loop for periodic LO disturbances. This reduction factor depends on the disturbance period, as seen by the $2\pi/T$ factor in (9). However, sensitivity to $\dot{y}_{\text{LO}}(t)$ is not restricted to periodic disturbances.

In fact, characterizing this $\dot{y}_{\text{LO}}(t)$ sensitivity solves an experimental mystery that occurred when we applied a large seemingly fixed drift rate to the LO of LITS, as shown in Fig. 12 (-5.1×10^{-9}/day), and surprisingly saw a slow drift of the output frequency, as shown in Fig. 13. Even though the output drift was reduced by almost five orders of magnitude to -1.4×10^{-13}/day, no such impact appeared in the simulations.

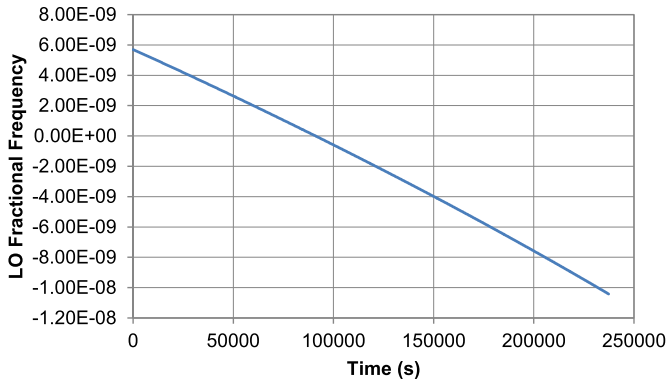

Fig. 12. LITS LO frequency versus time for a large drift rate -5.1×10^{-9}/day. The nonlinear drift component $\ddot{y}_{\mathrm{LO}} = -5.5 \times 10^{-10}$/day/day, obtained from a polynomial fit, is visible in the plot and gives an output drift of -9.9×10^{-14}/day, consistent with what would be needed to explain the induced output frequency drift shown in Fig. 13.

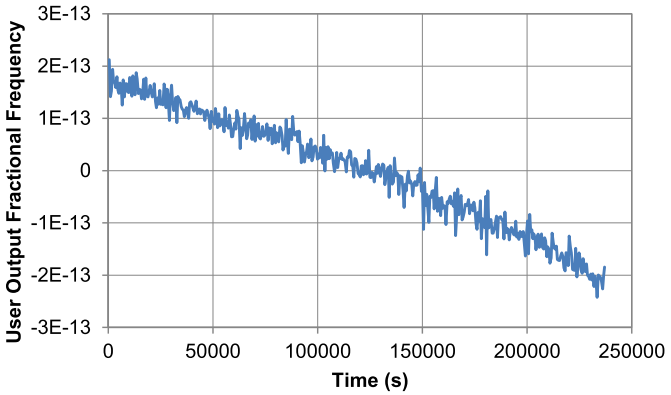

Fig. 13. LITS/VCXO User synthesizer frequency versus time, for the LO drift shown in Fig. 12. A linear regression gives a drift -1.4×10^{-13}/day. No drift compensation was implemented in the control loop for this test.

The explanation is that our applied "linear" USO drift had a small nonlinearity in it (visible in Fig. 12). This $\ddot{y}_{\mathrm{LO}}(t)$ was large enough, when multiplied by the 15.5-s sensitivity (nondrift compensated value), to produce the output frequency drift shown in Fig. 13. This test exemplifies that the ultimate long-term stability performance of the most stable Hg ion clocks (see [2] and [3]) could be limited by varying long-term drift and/or fluctuations resulting from a variable environment of the LO. What matters for clock stability using this type of control law is not necessarily how big or small the drift rate of the LO is, but rather, how stationary the LO drift rate is and the effectiveness of the implemented loop. *The takeaway is that the atomic-LO implementation can impact long-term clock stability independent of the long-term stability anticipated from the fundamental atomic sensitivities alone.*

D. Summary for Slow Frequency Disturbances

In summary, slow disturbances on any of the four subsystems shown in Fig. 2 propagate to the clock output as follows: User synthesizer, ion resonance, and 40-GHz synthesizer frequency disturbances, all propagate directly to the output frequency, although with the opposite sign for the 40-GHz synthesizer. LO/USO disturbances propagate with a reduction factor proportional to $dy_{\mathrm{out}}/d\dot{y}_{\mathrm{LO}}$—a sensitivity to LO-drift which is determined by the control loop algorithm. This sensitivity could be calculated based on control theory, but instead we demonstrate how to determine it experimentally and/or computationally. For the special case of periodic disturbances, the reduction factor is $2\pi/T$ times $dy_{\mathrm{out}}/d\dot{y}_{\mathrm{LO}}$ and the output fluctuation has a $-90°$ phase shift relative to the input disturbance. Note that we have used thermal disturbances in all the examples, but slow magnetic disturbances have similar impact. Table I summarizes the effect of these slow disturbances in the upper section of Column 2.

One consequence of the impact polarities is that equal fractional frequency disturbances on the 40 GHz and User synthesizers, which for the case of DSAC are colocated in the same instrument box, cancel each other out for these slow variations. So, even if these two synthesizers have (fractional frequency) sensitivities much larger than other sensitivities

TABLE I
SUMMARY OF IMPACTS TO CLOCK OUTPUT

Subsystem Being Disturbed	Slow Disturbance	Fast Disturbance During Rabi Interval	Fast Disturbance During Dead Time
User Synthesizer	1-1 impact	A) 1-1 impact, but averaged by measurement device response time.	A) 1-1 impact, but averaged by measurement device response time.
Ion Resonance	1-1 impact	B) Slow control loop impact. (Loop tries to track the frequency detected during each Rabi interval.)	None
LO/USO	Reduction factor proportional to $\frac{dy_{out}}{d\dot{y}_{LO}}$	A) 1-1 impact, but averaged by synthesizer and/or measurement device response time. B) Same slow control loop impact as for Ion resonance disturbance, but trying to counteract the disturbance rather than track it.	A) 1-1 impact, but averaged by synthesizer and/or measurement device response time.
40 GHz Synthesizer	-(Ion Resonance impact)	-(Ion Resonance impact)	None
40 GHz & User Synthesizer (common mode changes)	None	Fast 1-1 impact of User synthesizer is transmitted, but slower, common mode disturbance per Rabi interval is removed by control loop.	See User Synthesizer entry above.
40 GHz & User Synthesizer (differential changes)	1-1 impact	Fast 1-1 impact of User synthesizer is transmitted, as is slower differential disturbance per Rabi interval.	See User Synthesizer entry above.

All disturbances are assumed to be in fractional frequency, not phase. Phase disturbances must be converted to frequency before using the results of this table.

in the system, to the degree that they are equal and the two synthesizers experience the same slow thermal/magnetic environments, their impacts will cancel out. Table I notes this common mode cancelation and sensitivity to differential changes in the lower section of Column 2.

One final point is that this whole analysis focused on frequency disturbances as given by (1), but the main environmental sensitivity for synthesizers enters as a phase versus temperature or phase versus magnetic field impact. We can convert between periodic phase and frequency disturbances by taking a derivative, but note that it introduces a factor of $2\pi / T$ into the frequency sensitivity and shifts the ultimate clock disturbance by $-90°$ from the environmental disturbance.

VI. Paradigm for Understanding Impact of Fast Disturbances

A. Overview of Fast Disturbances

The analysis of fast disturbances is similar to that of slow disturbances with a few additional considerations. The main addition is attention to whether fluctuations occur while the microwaves are probing the ions or not (Rabi interval versus dead time). Table I contains two separate columns to describe fast fluctuations during each of these portions of the clock cycle (Columns 3 and 4). A second new aspect to consider is whether fluctuations are too fast to be detected by whatever device is measuring the output of the clock. The clock could, for example, end up tracking a disturbance at the millisecond-timescale, but such fluctuations are typically smoothed or subsampled when measured. Thus, the response time of the measurement device is noted where relevant in Column 3 and Column 4 entries.

As an overview of fast disturbances, we review impacts to the three relevant subsystems, the User synthesizer, ion resonance frequency, and LO/USO, this time focusing on whether the disturbance occurs during the Rabi interval or not.

First, we note that the User synthesizer is the one part of the system for which the timescale of the fluctuation and the interrogation cycle do not influence the output. This clock component is not within the control loop, so fluctuations propagate directly to the output. The User synthesizer row of Table I reflects this observation, showing a 1–1 impact on the output regardless of when fluctuations occur, but as mentioned, with some averaging introduced by the finite response time of the measurement device.

Next, we consider the ion resonance frequency (Row 2 of Table I). Because, this core frequency reference only impacts the output via the control loop, the only way disturbances on it enter is if they occur during the Rabi time, i.e., when the ion resonance is being probed. During each Rabi interval, the control loop compares the LO-based 40 GHz to the ion resonance frequency, but the measurement is only sensitive to frequency changes within each probe interval (weighted average). The Table I entry thus describes this impact as a slow control loop response that tracks the frequency detected during each Rabi interval. The long-term impact can be simple to evaluate if the disturbances are not changing from one Rabi interval to the next, or they can be much more complex if there is a slow modulation of disturbance size from cycle to cycle.

Finally, LO/USO disturbances cause a combination of the two impacts just discussed: A) the 1–1 fast impact that is tempered by the output measurement device as well as by the User synthesizer response time in this case and B) the slower control loop response that counteracts the disturbance during each Rabi interval. If the fluctuation during each Rabi interval is representative of the fluctuation during the dead time, and does not change from cycle to cycle, then the average disturbance on the output will be removed to the first order. However, if disturbances are more present in the Rabi interval, then the control loop will overcompensate, and if the disturbances are more present during the dead time, the control loop will undercompensate. This balance is a key to understanding fast USO disturbances. Examples will be given in subsection VI-B.

B. Case Study: Magnetorquers Shifting USO

For DSAC's flight demonstration experiment in low Earth orbit [5], [8], the primary fast disturbances come from the magnetorquers used for spacecraft maneuvering. We expect these to create a magnetic field of up to 1 G in the vicinity of the ion clock. They will fire every 4 s for varying durations between 0.25 and 0.5 s. They will also flip polarity every 49 min in tandem with the orbital period. Thus, we must account for the fast impulses they create on the four clock subsystems, as well as for the slower 98-min period modulation caused by the polarity flips.

We simulated the potential USO impact due to magnetorquers directly on the LITS/VCXO ground system as well as using the computer model. Both gave similar results, enabling a validation of this aspect of the model. The validation run injected 3.0×10^{-12} LO shifts occurring on a 7.1-s cadence, nearly resonant with the LITS/VCXO 7.0-s clock cycle time. We chose this slow magnetorquer cycle time in order to probe the impact of having it in close resonance with the clock cycle. Disturbance durations were uniformly distributed between 0.25 and 0.5 s, and determined by a random number generator. As well, the polarity of the disturbance was flipped every 49 min and Rabi times were 3.8 s. Drift compensation was not needed or used in this test.

Fig. 14 shows the computer model results. The LO ADEV is shown both with and without the disturbance (orange versus blue). The simulated ion clock and VCXO system output ADEV is shown in black. (Note that LO drift was added in both the modeled and experimental system to simulate a typical flight USO drift.) As expected from Table I, the short-term bump on the disturbed LO ADEV appears also on the output ADEV. The bump on the output ADEV at $\sim$150 s can be understood in terms of the slow migration of disturbance pulses from being all within Rabi intervals to being all within dead time intervals and then back to Rabi over the course of 70 cycles (490 s). This is due to the 0.1-s difference we orchestrated between the clock cycle time and the disturbance cycle time. From (6), we would expect an ADEV bump to

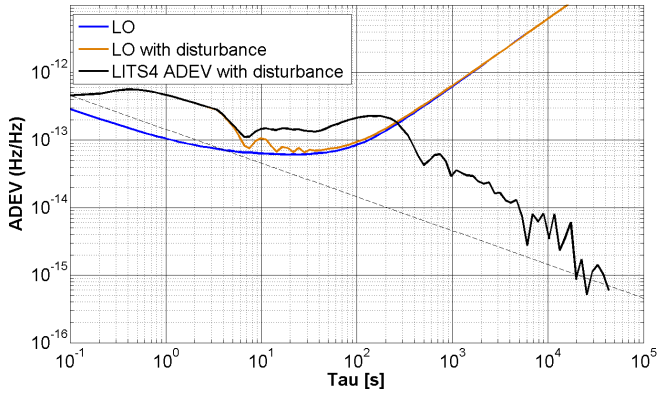

Fig. 14. Simulated LO (VCXO) input (blue and orange) and User Output (black) for LITS/VCXO clock system with magnetorquer disturbance. The straight line is the ADEV we would expect from signal to noise alone (no disturbances, Dick effect or other excess noise): $1.4 \times 10^{-13}/\sqrt{\tau}$ in this case.

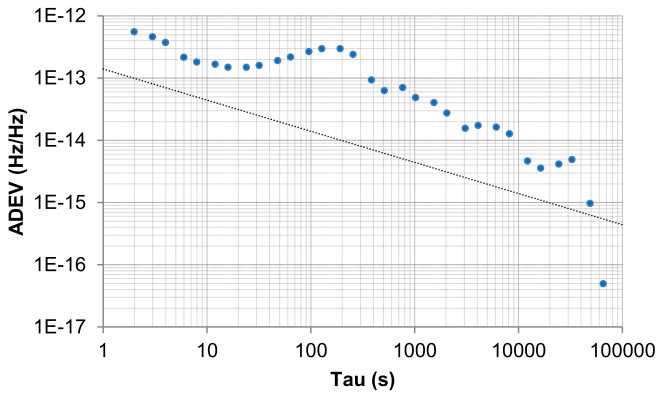

Fig. 15. Experimental output data (circles) for LITS/VCXO clock with disturbances on the LO designed to mimic the impact of magnetorquer pulses. The straight line is the ADEV we would expect from signal to noise alone (no disturbances, Dick effect or other excess noise): $1.4 \times 10^{-13}/\sqrt{\tau}$ in this case.

occur at 180 s for a 490-s sinusoidal disturbance, consistent with ∼150 s we visually observe in Figs. 14 and 15. Fig. 15 shows that the LITS/VCXO ground system results agree well with the simulated results of Fig. 14.

The amplitude of the 150-s ADEV bump in Figs. 14 and 15 can also be understood using the developed analytic paradigm. The longest duration (0.5 s) magnetorquer shifts cause the largest impact to the output frequency, so we focus on these to first predict/validate the envelope of the output fluctuations shown in Fig. 16 (simplified simulation omitting the 98-min period polarity flips).

The 0.5-s duration pulses only shift the LO for 0.5/7.1, i.e., 7% of the time. When they occur during the dead time, they do not induce any correction from the control loop, and thus shift the average output 7% of the actual disturbance size, or $+2.1 \times 10^{-13}$. This is consistent with the upper envelope of the frequency versus time plot shown in Fig. 16 and illustrates the use of Table I (LO/USO entry in "fast disturbance during dead time").

The lower edge of the envelope would result from this overall shift plus any control loop reaction

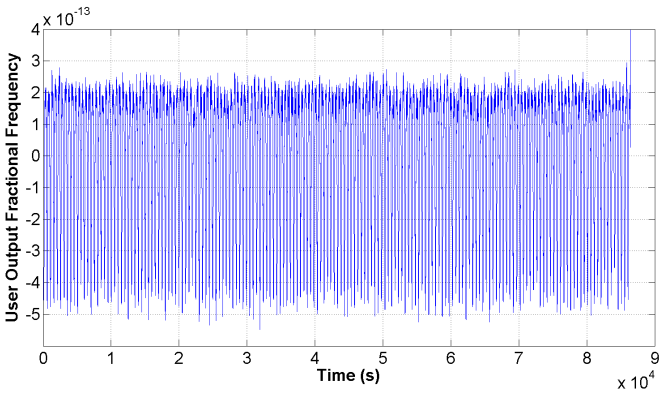

Fig. 16. Modeled User synthesizer frequency versus time for LITS/VCXO clock parameters with magnetorquer disturbances, but with no polarity reversals. User Output is smoothed with 100-s running average to eliminate most LO noise, leaving excursions mainly due to magnetorquers. (Envelope of excursions when no magnetorquers are included is 1×10^{-13}.)

(i.e., both LO entries in "fast disturbance during Rabi interval" column of Table I). When the 0.5-s duration pulses occur entirely during the Rabi interval, the control loop maximally compensates/overcompensates by reducing both synthesizers the perceived shift amount. If our algorithm used a simple frequency average to calculate each transition probability, this shift would be 0.5/3.8 = 13% of the actual disturbance (for our 3.8-s Rabi time). However, because of our sine-squared weighting function, the disturbance pulses at the center of the Rabi window cause an enhanced ion response and control loop correction of up to 26% or 7.8×10^{-13}. When subtracted from the overall $+2.1 \times 10^{-13}$, a lower envelope edge of -5.7×10^{-13} would be expected. (Note: Fig. 16 shows a lower edge of $\sim -4 \times 10^{-13}$, because the response time of the control loop and/or of the running average is not fast enough to reach the lower floor. However, if we change the magnetorquer cadence and fix the pulses to *always* be at the center of the Rabi interval, we do indeed observe the predicted -5.7×10^{-13} level.)

To use our analytic paradigm and predict the ADEV impact for our original scenario, we take somewhere between the observed peak-to-peak disturbance size in Fig. 16 and the expected size, i.e., $6 \times 10^{-13} \rightarrow 8 \times 10^{-13}$, plus (5), and arrive at an expected ADEV impact of $2.2 \times 10^{-13} \rightarrow 2.9 \times 10^{-13}$, consistent with the peaks of Figs. 14 and 15.

Fig. 17 shows the same simulated output frequency envelope when polarity flips are added back in. Note that these flips only appear visibly on the output because of the asymmetry of Fig. 16 about zero. Note also that the envelope of frequency excursions shown in Figs. 16 and 17 is sensitive to how much smoothing is performed. No smoothing allows too much LO noise to appear, and too much smoothing removes the resolution needed to see the 98-min period polarity flips and the full size of the magnetorquer influence. Different smoothing choices were tested, and 100 s was chosen as a good compromise between seeing the full excursions due to magnetorquers but keeping LO noise below a 1×10^{-13} contribution (15% of the visible scatter).

Further computer simulations showed the peak of the ADEV disturbance move to higher tau when the magnetorquer cycle

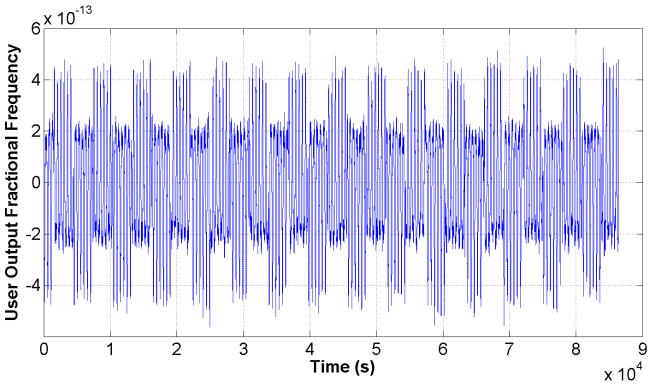

Fig. 17. Same as Fig. 16 but with polarity flips. Flips are visible because of the asymmetric nature of the shifts on the output.

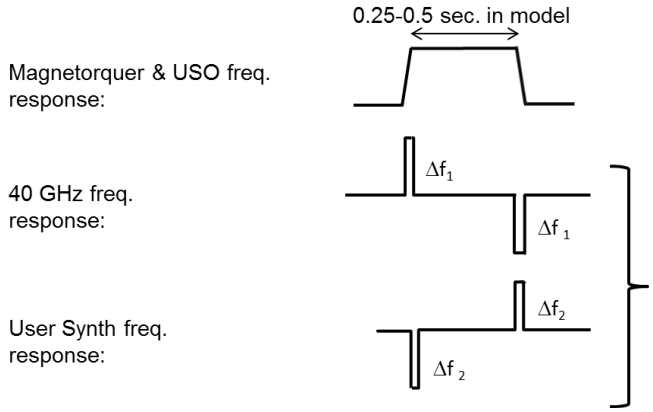

Fig. 18. Pictorial representation of magnetorquer impact on both synthesizers. $\Delta f = sensitivity * dB/dt$, where Δf is the frequency shift each synthesizer experiences as the magnetic field is ramping and *sensitivity* is the phase versus magnetic field sensitivity for each synthesizer.

time was shifted closer to resonance with the clock cycle, and move to lower tau and eventually disappear under the baseline ADEV when the magnetorquer cycle time was shifted farther from resonance, as expected. The height of the peak remained roughly the same when visible. In addition, as the disturbance peak approached 2200 s, the location we would expect for the 98-min period polarity flips, we saw interaction between these two phenomena: the cycle slippage and the polarity flips. The center of the disturbance peak caused by the cycle slippage reduced into a double peaked structure due to the polarity flips.

In summary, our paradigm for understanding fast and slow fluctuations enables a phenomenological description of how the magnetorquer-induced USO shifts impact the output ADEV, and how the relevant repetition rates (phasing) ultimately determine the impact. The computer simulations can be used to probe more exact parameter sets, but understanding the relationship between the two cycle times enables us to recommend that the DSAC's clock cycle time should not be chosen near a multiple of the 4-s magnetorquer repetition rate. Avoiding this type of cyclical resonance should prevent any magnetorquer impact on DSAC's longer term ADEV due to USO shifts, especially since shift magnitudes are expected to be much smaller than used for this validation run.

C. Case Study: Magnetorquers Shifting Synthesizers

Similar simulations can be performed to investigate the effect of magnetorquers on the synthesizers, however, because the synthesizer magnetic sensitivity causes a change in *phase* rather than *frequency*, the synthesizer only experiences a *frequency* disturbance at the beginning and end of each magnetorquer pulse (i.e., while the magnetic field is changing). Fig. 18 portrays this pictorially. The rate at which the magnetic field rises and falls is slowed dramatically in this picture to show the effect that synthesizer frequency shifts are proportional to dB/dt. For DSAC, the magnetic sensitivities of the two synthesizers happen to have opposite polarities, as depicted by opposite going responses in Fig. 18, and therefore, common mode magnetic disturbances on the two synthesizers are less likely to cancel. However, for each magnetorquer pulse, there is a positive and a negative frequency shift to each synthesizer, so to the extent that the magnetic field amplitude starts from and returns to the same baseline, much cancelation can still occur. Still, for the 40 GHz synthesizer, this relies on the entire pulse being situated within a Rabi or dark period.

VII. Conclusion

In summary, we have presented a paradigm for analyzing the impact of disturbances to each part of the frequency chain for a generic atomic clock system. We explained fast as well as slow disturbances and conclude which ones are filtered out by the control loop and to what degree, as summarized in Table I. We validated our analytic estimates with computer and/or experimental simulations, and of note, presented example results of LO disturbances in the form of drift, 98-min variations, and random-duration magnetorquer firings. We point out a crucial sensitivity to changing LO drift rate, which has implications for long-term stability of a variety of atomic clock implementations. This paper will enable future trade space discussions to determine which types of LOs are best paired with which types of atomic references to achieve the long-term system results desired.

References

[1] R. L. Tjoelker *et al.*, "A mercury ion frequency standard engineering prototype for the NASA deep space network," in *Proc. 50th IEEE Annu. Int. Freq. Control Symp. (IFCS)*, Honolulu, HI, USA, Jun. 1996, pp. 1073–1081.

[2] E. A. Burt, W. A. Diener, and R. L. Tjoelker, "A compensated multi-pole linear ion trap mercury frequency standard for ultra-stable timekeeping," *IEEE Trans. Ultrason., Ferroelect., Freq. Control*, vol. 55, no. 12, pp. 2586–2595, Dec. 2008.

[3] E. A. Burt, L. Yi, B. Tucker, R. Hamell, and R. L. Tjoelker, "JPL ultra-stable trapped ion atomic frequency standards," *IEEE Trans. Ultrason., Ferroelect., Freq. Control*, vol. 63, no. 7, pp. 1013–1021, Jul. 2016.

[4] R. L. Tjoelker *et al.*, "Mercury atomic frequency standard development for space based navigation and timekeeping," in *Proc. 43rd Precise Time Time Interval (PTTI)*, Long Beach, CA, USA, Nov. 2011, pp. 293–304.

[5] R. L. Tjoelker *et al.*, "Mercury ion clock for a NASA technology demonstration mission," *IEEE Trans. Ultrason., Ferroelect., Freq. Control*, vol. 63, no. 7, pp. 1034–1043, Jul. 2016.

[6] *DSN Telecommunications Link Design Handbook, Publication 810-005, Module 304 Revision B*, Jet Propulsion Laboratory, California Institute of Technology, Pasadena, CA, USA, Dec. 2014.

[7] J. D. Prestage and G. L. Weaver, "Atomic clocks and oscillators for deep-space navigation and radio science," *Proc. IEEE*, vol. 95, no. 11, pp. 2235–2247, Nov. 2007.
[8] T. A. Ely *et al.*, "The deep space atomic clock mission," in *Proc. 23rd Int. Symp. Space Flight Dyn.*, vol. 2. Pasadena, CA, USA, Oct. 2012, pp. 1–15.
[9] G. J. Dick, "Local oscillator induced instabilities in trapped ion frequency standards," in *Proc. 19th Precise Time Time Interval (PTTI)*, Redondo Beach, CA, USA, 1987, pp. 133–147.
[10] G. J. Dick, J. D. Prestage, C. A. Greenhall, and L. Maleki, "Local oscillator induced degradation of medium-term stability in passive atomic frequency standards," in *Proc. 22nd Precise Time Time Interval (PTTI)*, Vienna, VA, USA, 1990, pp. 487–508.
[11] D. A. Stowers, R. L. Sydnor, R. L. Hamell, M. J. Grimm, and G. J. Dick, "Digital frequency-lock loop using high-resolution TAC and advanced control algorithm for trapped-ion frequency standards," in *Proc. 49th Annu. Int. Freq. Control Symp. (IFCS)*, vol. 2. San Francisco, CA, USA, May 1995, pp. 212–216.
[12] W. Hurewicz, "Filters and servo systems with pulsed data," in *Theory of Servomechanisms, MIT Radiation Laboratory Series*, vol. 25, H. M. James, N. B. Nichols, and R. S. Phillips, Eds. New York, NY, USA: McGraw-Hill, 1947, ch. 5, pp. 231–261.
[13] G. F. Franklin, J. D. Powell, and A. Emani-Naeini, *Feedback Control of Dynamic Systems*, 5th ed. Upper Saddle River, NJ, USA: Prentice-Hall, 2006, ch. 8.
[14] C. Audoin, G. Santarelli, A. Makdissi, and C. Clairon, "Properties of an oscillator slaved to a periodically interrogated atomic resonator," *IEEE Trans. Ultrason., Ferroelect., Freq. Control*, vol. 45, no. 4, pp. 877–886, Jul. 1998.
[15] W. J. Riley, "Handbook of frequency stability analysis," NIST, U.S. Dept. Commerce, Boulder, CO, USA, Tech. Rep. 1065, Jul. 2008.

Daphna G. Enzer received the S.B. degree in physics from Yale University, New Haven, CT, USA, in 1989, and the A.M. and Ph.D. degrees in atomic physics from Harvard University, Cambridge, MA, USA, in 1991 and 1996, respectively. Her Ph.D. thesis focused on the quantum to classical transition of a single electron in a Penning trap.

After a one-year post-doctoral fellowship at Harvard University, she spent two years as a Director's Post-Doctoral Fellow at Los Alamos National Laboratory working on quantum computing with trapped calcium ions and quantum cryptography with polarization-entangled photon pairs. She joined the NASA Jet Propulsion Laboratory, California Institute of Technology, Pasadena, CA, USA, in 2001, and is currently a member of the Frequency and Timing Advanced Instrument Development Group. Her interests include precision measurement instruments, both development and data analysis, with contributions to: cold atom cesium fountain and space clock prototype development; Gravity Recovery and Interior Laboratory (GRAIL) mission radio link performance analysis; and JPL frequency stability measurement-system development, algorithms, and performance analysis. She is currently leading mercury ion clock system modeling and evaluation activities and supports several areas of the Deep Space Atomic Clock (DSAC) Mission.

Dr. Enzer is a member of the American Physical Society.

William A. Diener received the A.A. degree in aircraft maintenance from the Glendale College, Glendale, CA, USA, in 1973.

He was with American Jet, Van Nuys, CA, USA, Continental Airlines, Los Angeles, CA, USA, and Western Airlines, Los Angeles, CA, USA, until 1982. In 1982, he joined the Frequency Standards Laboratory, NASA Jet Propulsion Laboratory (JPL), California Institute of Technology, Pasadena, CA, USA. He currently leads low noise oscillator, atomic frequency standard, clock, signal distribution, and time transfer performance and environmental test activities in JPL's Frequency Standards Test Laboratory (FSTL) and is responsible for the hydrogen maser reference standards and calibration with JPL and in the NASA Deep Space Network.

David W. Murphy received the B.A. degree (Hons.) in physics from the University of Cambridge, Cambridge, U.K., in 1983, and the Ph.D. degree in physics from The University of Manchester, Manchester, U.K., in 1988. His Ph.D. in physics (radio astronomy) was on VLA observations of core-dominated quasars.

From 1987 to 1988, he was a Research Associate with The University of Manchester. From 1989 to1990, he was a National Research Council Post-Doctoral Associate at the Jet Propulsion Laboratory (JPL), California Institute of Technology, Pasadena, CA, USA. In 1991, he became a member of JPL's Astronomical Measurements Group, and in 2006 its Group Supervisor. From 1991 to 2011, he was involved in both the Japanese VSOP and the Russian RadioAstron Space VLBI missions and NASA's Space Interferometry Mission and Kepler mission. In 2011, he joined the Deep Space Atomic Clock (DSAC) Project and in 2012 became the Group Supervisor of the Near Earth Tracking Applications Group. His DSAC mission work involves using the data from the on-board GPS receiver to determine the Allan Deviation of the DSAC clock.

Shanti R. Rao received the Ph.D. degree in physics from the California Institute of Technology, Pasadena, CA, USA, in 2003.

He is currently a Senior Engineer with the Instruments Division, Jet Propulsion Laboratory, California Institute of Technology.

Robert L. Tjoelker (M'98–SM'05) received degrees in physics, mathematics, and architecture from the University of Washington, Seattle, WA, USA, and the Ph.D. degree in physics from Harvard University, Cambridge, MA, USA, with a focus on a precision comparison of the proton and antiproton mass.

He was an Inaugural Member of the Trapped Antiproton Collaboration from 1985 to 1990. From 1988 to 1990, he resided with the European Laboratory for Particle Physics (CERN), Geneva, Switzerland, where he performed a series of confinement, cooling, and precision measurements with antiprotons in an ion trap. In 1990, he joined the Frequency Standards Laboratory, NASA Jet Propulsion Laboratory, California Institute of Technology, Pasadena, CA, USA. He is currently a Principal Member of the Technical Staff and Group Supervisor of the Frequency and Timing Advanced Instrument Development Group. He and his group develop high-stability mercury trapped ion frequency standards, state-of-the-art atomic clocks and timing systems, and photonic reference distribution systems for space missions and the NASA Deep Space Network. He is currently co-investigator of the Deep Space Atomic Clock (DSAC) mission.

Dr. Tjoelker is a member of the American Physical Society, the IEEE, and the Institute of Naviagion (ION).